Journal of Hazardous Materials 505 (2026) 141549

Contents lists available at ScienceDirect

Journal of Hazardous Materials

journal homepage: www.elsevier.com/locate/jhazmat

Polyester microplastic fibers rearrange soil physical quality indicators without compromising hydraulic function in six Mediterranean soils: Insights from S-theory indicators

Rosolino Ingraffia *, Cristina Bondì, Dario Autovino, Dario Giambalvo, Paolo Ruisi, Vincenzo Bagarello, Massimo Iovino *

Department of Agricultural, Food and Forest Sciences, University of Palermo, Palermo 90128, Italy

HIGHLIGHTS

- The choice of SWRC model influenced estimation of SPQ inflection point indicators.
- PES MP contamination altered soil pore architecture but not capacitive indicators.
- Inflection point indicators provide sensitive diagnostics for PES MP impacts.
- The most detectable SPQ modifications occurred at 1 % contamination level.
- Texture-specific responses require soil-type-based risk assessment strategies.

GRAPHICAL ABSTRACT

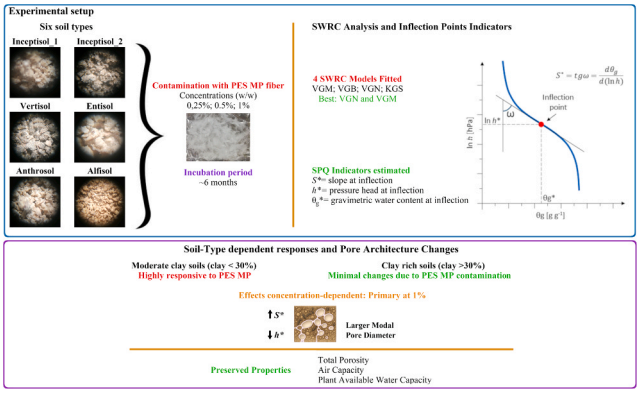

ARTICLE INFO

Keywords:
Microplastics
Soil physical quality
Water retention curve
S-index
Polyester fibers
Microplastic in agroecosystem

ABSTRACT

Microplastics contamination in agricultural soils represents an emerging threat to soil health and ecosystem functioning. This study investigated the effects of polyester (PES) microplastic (MP) fibers on soil physical quality (SPQ) using indicators derived from soil water retention curve (SWRC) inflection point, based on Dexter's S-theory. Six soils with different textures were contaminated with PES fibers at concentrations of 0.25 %, 0.5 %, and 1 % (w/w) and incubated for about six months. Four SWRC models (van Genuchten with Mualem constraint, VGM; van Genuchten with Burdine constraint, VGB; van Genuchten unconstrained, VGN; and Kosugi, KSG) were fitted to experimental water retention data. The VGN and VGM models provided the best fitting accuracy across soil types. Overall, MP contamination altered key SPQ indicators determining: a decrement of the pressure head at inflection point (h^*) and of effective porosity (Φ^*), indicating larger modal pore diameters; an increment of the slope at inflection point (S^*), suggesting enhanced soil aggregation. Effects were soil type and concentration dependent, with changes primarily occurring at 1 % MP concentration. Soils with moderate clay content (clay < 30 %) showed improved S^* values, while clay rich soils showed minimal response. Capacitive indicators (air capacity and plant available water capacity) remained largely unaffected, suggesting preserved total porosity

* Corresponding authors.
E-mail addresses: rosolino.ingraffia@unipa.it (R. Ingraffia), massimo.iovino@unipa.it (M. Iovino).

https://doi.org/10.1016/j.jhazmat.2026.141549
Received 24 October 2025; Received in revised form 13 January 2026; Accepted 18 February 2026
Available online 19 February 2026

despite internal pore structure modifications. These findings demonstrate that PES MP fiber contamination can alter soil pore architecture and aggregation without substantially impacting bulk hydraulic properties, highlighting the complexity of MP-soil interactions and the value of inflection point indicators for detecting subtle changes in soil physical quality.

1. Introduction

Soil quality is the result of an intricate interplay between soil chemical, biological, and physical aspects that synergistically influence the soil's ability to support plant life and play a central role in several environmental processes [1]. In agricultural soils it directly influences root development, water and nutrient availability, and ultimately crop productivity.

The physical quality of an agricultural soil is assessed primarily with reference to the mechanical and hydraulic characteristics in the crop root zone [2]. In particular, the soil's ability to retain and transmit water and air is a critical factor for healthy root function and plant growth. Several indicators have been proposed to quantify the level or degree of soil physical quality (SPQ) including relative bulk density, organic carbon content, saturated hydraulic conductivity, structural stability index, as well as pore size distribution and capacity-based indices derived from the soil water retention curve (SWRC) [1,3–7].

Dexter [8–10] proposed an index of SPQ, S^*, which is related to many important soil properties or conditions including organic matter content, hydraulic conductivity, compaction, tillage suitability, penetration resistance, plant-available soil water, root growth, and soil structural stability [11,12]. The S^*-index is defined as the slope of the soil water release curve at the inflection point when the curve is expressed as gravimetric water content versus natural logarithm of pore water pressure potential expressed in hPa. Dexter's analysis assumes that, in a drainage process from saturated condition, the pores that empty to the inflection point of the SWRC are predominantly the structural ones while, for soil drying below the inflection point, textural pores dominate [13]. Optimal S^* values have been suggested by Dexter [10], Dexter and Czyz [12], and Tormena et al. [14]. Although S^* can theoretically assume all values between 0 and ∞ , agricultural soils tend to fall within the range $0.007 \leq S^* \leq 0.14$ [12]. The S^*-theory has been widely applied across agricultural, forest, and environmental contexts [14–19] demonstrating consistent sensitivity to structural modifications induced by tillage systems, soil amendments, and environmental stressors [20–28].

While the slope of the water retention curve at the inflection point can be measured directly from water retention data, models such as the van Genuchten [29] or Kosugi [30] functions provide more objective and repeatable determinations [8], yielding inflection point indicators of SPQ (S^*, pressure potential h^*, gravimetric water content θ_g^*, effective porosity Φ^*, and pore-size distribution index λ^*) that characterize key aspects of soil pore structure. Details on determination of inflection point indicators of SPQ are provided in the Appendix. Changes in soil pore distribution arrangements due to external factors (tillage, compaction, salinity, organic and inorganic amendments) are expected to affect the SWRC and thus the related estimation of the inflection SPQ indicators. However, the choice of SWRC model can also influence the estimated inflection point indicators and thus the assessment of the SPQ. While model effects on SWRC fitting have been evaluated [31], the influence of SWRC model selection on the estimation of S^* and related inflection point indicators remains largely unexplored, representing a knowledge gap for comparative SPQ studies.

In recent years, the accumulation of microplastics (MPs; i.e., plastic particles < 5 mm; [32]) in agricultural soils has emerged as a potential threat to soil health, with documented effects on physical properties including bulk density, water holding capacity, porosity, hydraulic conductivity, and susceptibility to erosion [33–37]. However, the nature and magnitude of these effects vary substantially depending on polymer type, particle shape, and soil characteristics, highlighting the need for polymer-specific and texture-specific investigations. Agricultural soils MP contamination originates from multiple pathways, each characterized by distinct polymer profiles. Plastic mulching films predominantly introduce polyethylene and polypropylene, whereas organic amendments, including compost, biosolids, and wastewater-derived materials, represent an increasingly important contamination pathway with markedly different polymer composition [38–41]. In systems receiving organic amendments, fibrous MPs are often dominant, with polyester (PES) fibers consistently reported among the most abundant fiber types due to their high release from textile washing and subsequent transfer through wastewater treatment systems [39–42]. As organic amendment application expands globally, this PES-dominated pathway represents a growing environmental concern. Moreover, among the various types of MPs, PES MP fibers have been frequently observed to have distinct and texture-dependent effects on soil properties [34,35,37,43,44]. de Souza Machado et al. [37] showed that PES MP fibers markedly increased water holding capacity in a loamy sand soil whereas other MP types (polyacrylic fibers, polyamide beads and polyethylene high-density fragments) did not elicit similar effects. Ingraffia et al. [35] found that MP PES fibers did not affect total porosity, but slightly decreased microporosity and increased macroporosity. Similar effects were also observed by Zhang et al. [45], who ascribed the increment of soil macroporosity to an increased soil aggregation status. More recently, Chen et al. [43] reported that PES MP fibers improved aggregate stability in sandy loam soil, but slightly reduced it in clay loam, with variable effects across soil texture. Yet, PES treatments consistently reduced root biomass in the three soils, closely mirroring the biomass loss observed by Ingraffia et al. [35]. These divergent outcomes highlight that the physical and agronomic effects of PES MP fibers depend critically on soil texture, mineralogy, and intrinsic aggregation potential. A recent study by Neubert et al. [44] further confirmed this texture-dependency, showing PES MP fibers increased saturated hydraulic conductivity in silt loam soils but reduced it in sand, by creating preferential flow paths or clogging pores, respectively.

Placing these polymer-specific effects into an environmental context requires consideration of both current microplastic occurrence in agricultural soils and their projected long-term accumulation. While most field studies report microplastic contamination in terms of particle abundance, the few available mass-based estimates indicate that current microplastic levels in agricultural soils typically remain below 0.01 % w/w, though localized accumulation can reach 0.14 % w/w [38]. However, projection models indicate that total microplastic concentrations in agricultural systems could approach 0.7 % w/w within the next century [46], highlighting the need to investigate microplastic effects at contamination levels that may represent future accumulation worst-case scenarios. While these projections represent total microplastic loads, PES MP fibers can serve as a model polymer for investigating concentration-dependent effects on soil physical quality due to their prevalence in the expanding organic amendment pathway, their demonstrated texture-specific effects on soil properties, and their fibrous morphology which is among the most abundant microplastic shapes in organic amendments.

Given the observed complexity and variability in MP effects, particularly those of PES fibers across different soil types, a more integrated approach is needed to detect meaningful structural changes that standard metrics may overlook. SPQ indicators, specifically those associated with the SWRC inflection point, offer an integrated approach to assess MP effects on SPQ. To the best of our knowledge, the influence of

MP pollution on inflection point indicators of SPQ has not been assessed so far, representing a critical knowledge gap for understanding MP effects on soil health and ecosystem functions. Critically, it remains unclear whether these indicators retain their diagnostic value and interpretability under MP contamination, or if polymer-induced structural alterations fundamentally compromise their application in contaminated soils. Given the documented texture-dependency of PES effects on aggregate stability, porosity distribution, and hydraulic conductivity [35,43–45], we hypothesized that inflection point indicators would exhibit texture-specific sensitivity to PES contamination, with coarse-textured soils low in organic carbon showing greater responsiveness than clay-rich soils or those with higher organic matter content.

The main aim of this study was to assess the influence of PES MP fiber pollution on inflection point indicators of SPQ across six Mediterranean soil types differing in texture and mineralogy. The fitting accuracy of four SWRC models was preliminarily assessed and the S^*-theory applied to estimate the inflection SPQ indicators. These indicators were then interpreted in terms of their agronomic and ecological significance. This study offers a novel diagnostic approach for detecting how PES MP fiber contamination alters pore structure and provides a practical tool for soil health monitoring and risk assessment within agroecosystems.

2. Materials and methods

2.1. Selected soils and sample preparation

Six soils with different textures were collected from the upper 30 cm of the soil profile from designated sampling areas across Sicily, within a typical Mediterranean environment in southern Italy (sampling coordinates are reported in Table 1). Mediterranean agricultural soils are characterized by moderate to low organic matter content and seasonal wetting-drying cycles that influence structural stability and aggregation, making pore architecture critical for water management under semi-arid conditions. The six selected soils represent a range of soil types common across Mediterranean agricultural landscapes, covering diverse textural classes and physicochemical characteristics. Vertisol, Entisol, and Alfisol were selected based on their widespread distribution in Mediterranean regions and their contrasting physical properties, as previously characterized by Ingraffia et al. [34]. Two Inceptisols with different clay contents (Inceptisol_1: loam texture; Inceptisol_2: clay loam texture) were included to represent intermediate textural classes commonly found in Mediterranean croplands, allowing assessment of MP effects across a textural gradient. The Anthrosol represents a distinctive human-modified soil type characteristic of particular agricultural systems, as described by Dazzi et al. [47]. Together, these six soils encompass a textural range from loam to clay, with clay content varying from 15 % to 41 % (Table 1).

After sampling, the soils were air-dried, sieved through a 600 μm mesh, and stored at 4°C until the experiments commenced, approximately two months later. This procedure was implemented to minimize alterations to the natural microbial community. At the time of sampling, the six soils were visually verified to be free from meso- and macroplastic particles contamination. Analytical procedures to assess the contamination of smaller plastic particles were not conducted; therefore, it cannot be excluded that the control treatments may have contained detectable amounts of micro- and/or nanoplastic particles. The soils were classified according to the United States Department of Agriculture (USDA) classification and characterized using the following methods: particle size distribution [48], total nitrogen (TN; Kjeldhal), total organic carbon (TOC; Walkley–Black), pH, saturated electrical conductivity at 25°C (EC), and cation exchange capacity (CEC). The main physicochemical properties of the soils are reported in Table 1.

PES fiber was selected as a model MP type due to its prevalence in organic amendment-derived contamination and documented texture-specific effects on soil physical properties [34,35,37,39–42]. To induce PES MP fibers contamination, a 100 % PES white rope (Marlow, Marlowbraid classic Rope) was manually cut to generate secondary MP fibers. These fibers were analyzed by scanning a minimum of 200 fibers on PVC trays ten times (Epson Perfection V800 scanner, 8 bit grayscale, 800 dpi), followed by image analysis using WinRHIZO (WinRHIZO Pro v. 2007d, Regent Instrument Inc., Quebec, Canada). The mean fiber length and standard deviation, SD, were 2.87 mm and 0.31 mm, respectively. Fiber morphology and dimensional characteristics were further analyzed using scanning electron microscopy (SEM; Phenom XL, Thermo Fisher Scientific). SEM analysis revealed cylindrical fibers with a mean diameter of 30 ± 3 μm, relatively smooth surfaces, and predominantly straight orientation. The solid, compact internal structure observed in fiber cross-sections indicates high structural rigidity, which may influence fiber-soil mechanical interactions. Representative SEM images are provided in supplementary materials (Fig. S1).

The selected MP concentrations (0.25 %, 0.5 %, and 1 % w/w) were based on previous studies reporting significant changes in soil biophysical environment and plant response [34–37,49]. Moreover, while current microplastic levels in agricultural soils typically remain below 0.01 % w/w [38], projection models indicate that MP concentrations could approach 0.7 % w/w within the next century [46]. The experimental range therefore enables detection of concentration-dependent effects on soil physical quality across contamination trajectories. To contaminate the soil, the fibers were added to a blender (Waring® WSG30; Waring Commercial, Torrington, Connecticut, USA) as a band sandwiched between two layers of soil, and the mixture was blended five times for 5 s each to ensure a more homogeneous distribution of the fibers throughout the soil. The same procedure was applied to the six soils of the control treatment, i.e., 0 % w/w of MP (for details see [34,35]).

The control was performed in eight replicates, whereas the PES MP addition treatment was conducted in four replicates. Unbalanced replication was used to optimize statistical power for treatment vs control comparisons while minimizing experimental units, as the control group serves as the common baseline for all treatment comparisons and

Table 1
Main physical and chemical characteristics of the selected soils.

Soil	Inceptisol_1	Inceptisol_2	Vertisol	Entisol	Anthrosol	Alfisol
Pedon	Vertic Haploxerept	Vertic Xerochrept	Typic Haploxerert	Typic Xerorthent	Pantoterric Anthrosol	Typic Rhodoxeralfs
Classification	Loam	Clay loam	Clay	Loam	Silt loam	Loam
Site coordinates	37.539583°N,13.518861° E	37.541861°N, 13.515861° E	37.556140° N, 13.515400° E	37.561368° N, 13.512904° E	37.169083°N, 13.783306°E	37.643511° N, 12.628327° .E
Soil use	Arable land	Arable land	Arable land	Arable land	Permanent Crop	Arable land
Clay (%)	14.9	31.7	41.4	20.9	23.4	15.2
Silt (%)	39.0	41.7	35.7	46.1	51.2	43.1
Sand (%)	46.1	26.6	22.8	33.0	25.4	41.7
TN (g Kg^{-1})	0.90	1.80	1.54	1.20	0.78	0.77
TOC (g Kg^{-1})	6.3	16.8	15.8	9.3	3.0	11.2
pH (-)	7.1	7.2	7.7	7.8	8.1	7.6
EC (dS m^{-1})	1.9	2.2	1.9	1.9	-	2.01
CEC (cmol kg^{-1})	26.8	35.0	30.0	18.4	12.0	13.8

benefits from increased precision. Therefore, overall, 120 samples were prepared, resulting from 8 control samples +12 contaminated samples (3 concentrations × 4 replicated samples) ×6 soils. Samples were obtained by compacting the dry mass of each soil into cylinders with a diameter and height of 5 cm. Following preparation, the 120 soil samples were watered by capillarity and then placed in a growth chamber, kept in the dark, and maintained at 23 ± 2°C temperature and 60 ± 5 % relative humidity of for approximately 6 months. Throughout the incubation period, the soil samples were irrigated twice a week to a moisture content close to the field capacity. After each irrigation, the samples were re-randomized to exclude any possible artifact due to a non-uniform treatment. The six-month incubation period was chosen to allow for soil structure stabilization and microplastic integration into the soil matrix, ensuring equilibrium conditions before analysis.

2.2. Soil water retention curve measurements

The SWRC was determined experimentally using the hanging water column apparatus [50] for higher pressure potential values, h (m), ranging from −3 to −100 cm, and the plate extractor method [51] for lower potentials, with h values ranging from −100 to −15,000 cm. In the hanging water column method, the soil sample was placed on the surface of the porous plate of a glass funnel and was saturated from below through three successive 24-hour steps of equilibrium at the potentials of −20, −10, and −5 cm, followed by submersion (i.e., $h = 0$) for 2 h.

Starting from saturated conditions, the soil samples underwent desorption by applying a sequence of eight progressively decreasing h values: −3, −5, −10, −20, −30, −50, −70, and −100 cm. At each equilibrium h value, the drained water volume was collected into a burette and recorded. The gravimetric water content, θ_g (g g^{-1}), at each equilibrium stage was obtained by adding the drained weight of water to the value determined at the end of the drainage sequence ($h = -100$ cm) by weighing the sample after oven-drying at 105 °C for 24 h. Subsequently, the dry soil of each sample was crushed and three replicated samples were prepared by packing 25-g-mass of soil into cylinders having a diameter of 5 cm and a height of 1 cm at the same bulk density as measured in the larger samples. Gravimetric water content corresponding to $h = -100$, −330, −1000, −3300, and −15,000 cm was then determined using a pressure plate apparatus. The determination of θ_g at $h = -100$ cm was included in the pressure plate experiments to facilitate comparison with the θ_g value measured at the same potential using the tension apparatus. All analyses were conducted in the laboratory under temperature-controlled conditions of 22 ± 1 °C. Where needed, the gravimetric water content θ_g were converted into the corresponding volumetric ones, θ (m^{3}m^{-3}), using the dry bulk density of each sample measured at $h = -100$ cm.

2.3. Data analysis

Four unimodal SWRC models were considered to fit the experimental $\theta_g(h)$ data, namely the van Genuchten model (eq. A.2 of the Appendix) with fixed relationships between n and m parameters in the form of $m = 1 - 1/n$ (VGM; [52]), $m = 1 - 2/n$ (VGB; [53]) or with no fixed relationship between n and m parameters (VGN), and the Kosugi (KSG) model (eq. A.8). Using a fixed relationship between n and m reduces the flexibility of eq. (A.2) whereas more accurate results can be obtained by leaving n and m parameters unconstrained [54]. For simplicity, the absolute value of h was used when fitting the SWRC models to the $\theta_g(h)$ data and estimating the corresponding SPQ indicators.

The Solver® add-in (Frontline Systems, Incline Village, NV) of Excel® (Microsoft Corporation, Redmond, WA) was used to fit the four SWRC models. The selected Solver options included the generalized reduced gradient optimization method and central difference derivatives. The fitting accuracy of the different SWRC models to the measured data was assessed using the coefficient of determination (R^2), the root mean square error (RMSE) and the Akaike's information criterion (AIC) [31]. The AIC was used to account for the trade-off between model fit and model complexity. A better model fit is indicated by a higher R^2 value and lower RMSE and AIC values. To compare model performance at different applied pressure heads, the RMSE values were normalized (nRMSE) by dividing them by the mean of the measured θ_g values at each given h value.

Equations for estimation of the inflection SPQ indicators are listed in Appendix (eqs. A.3-A.7 for the van Genuchten model and eqs. A.10-A.12 for Kosugi model). For each SWRC model, the widely used capacitive indicators of SPQ accounting for the soil's ability to store and provide air and water to the crops were also calculated [55]. The air capacity, AC (cm^3 cm^{-3}), was calculated as the difference between the volumetric soil water content at saturation and at field capacity ($h = -100$ cm). The plant available water capacity PAWC (cm^3 cm^{-3}), was calculated as the difference between the volumetric soil water content at field capacity and at permanent wilting point ($h = -15000$ cm) [1].

The distribution of the SPQ data was initially evaluated using the Lilliefors test [56], considering both a normal (NO) and a ln-normal (LNO) distribution. Because several SPQ indicators violated the normality assumption, a non-parametric factorial analysis was performed using the Aligned Rank Transform (ART) implemented via the ARTool package [57], enabling non-parametric factorial ANOVA with interaction testing while maintaining interpretability in a linear model framework. ART-based ANOVAs were applied separately to each investigated SPQ indicator followed by post-hoc pairwise comparisons with multiplicity adjustment to identify which levels differed.

The effects of MP contamination, soil type, and their interaction on SPQ indicators was assessed using ART. Following the ANOVA, the magnitude and direction of MP impacts within each soil type were quantified using accelerated bootstrap resampling to estimate mean differences (Δ) between each treatment and the corresponding control and the corresponding 95 % confidence intervals (CIs) with the "boot" package [58]. These Δ estimates are reported in figures and annotated directly on the SPQ indicator plots. Data visualization was performed using the "tidyverse" meta-package [59] which include "ggplot2" [60]. All analyses were conducted in R version 4.4.2 [61].

3. Results and discussion

3.1. Model performance evaluation

Considering the entire dataset ($N = 1434$), the best performance in terms of fitting the $\theta_g(h)$ data was obtained by the VGN model and the worst by the VGB model. Intermediate results were obtained with VGM and KSG (Fig. S2 and S3). All the statistics considered to assess the fitting accuracy of the SWRC models (R^2, RMSE and AIC) concurrently classified the performance of the models in the order VGN > VGM > KSG > VGB (Table 2). Despite having one additional parameter, the VGN model achieved lower AIC value than the 4-parameter models (VGM, VGB, KSG), indicating superior overall performance. The ART ANOVA confirmed that model, soil type, and MP contamination all exert strong effects on RMSE. The analysis also revealed effects of the two-way interactions, whereas no effect was observed on the three-way (Table S1).

Separately considering the fitting for the six soils, the models yielded R^2 values between 0.978 and 0.996, RMSE values between 0.0059 and 0.0173, and AIC values ranging from −1.92 to −1.34 (Table 2). On average, the lowest values of RMSE and AIC were obtained for Inceptisol_1 and the highest for Vertisol. The coefficients of determinations R^2 were maximum for Entisol and minimum for Alfisol. However, for a given soil, the performance of the four SWRC models was relatively similar. The ratio between the lowest and the highest RMSE values obtained with the different SWRC models ranged from 0.70 (Entisol) to 0.83 (Vertisol) thus indicating that an inappropriate selection of the model could yield a worsening of the water content prediction by an average factor of approximately 1.3. Differently, the fitting goodness was greatly affected by the soil type. For a given model, the ratio

Table 2
Fitting statistics for the considered SWRC models.

	SWRC model			
	VGM	***VGB***	***VGN***	***KSG***
	All data N = 1434			
R^2	0.994	*0.993*	**0.995**	0.993
RMSE	0.0101	*0.0114*	**0.0097**	0.0110
AIC (x1000)	-9.88	*-9.48*	**-9.99**	-9.61
	Inceptisol_1 - N = 240			
R^2	0.992	*0.990*	**0.994**	0.992
RMSE	0.0067	*0.0075*	**0.0059**	0.0067
AIC (x1000)	-1.85	*-1.79*	**-1.92**	-1.86
	Inceptisol_2 - N = 240			
R^2	0.993	*0.990*	**0.995**	0.993
RMSE	0.0078	*0.0093*	**0.0069**	0.0079
AIC (x1000)	-1.77	*-1.68*	**-1.84**	-1.77
	Vertisol - N = 236			
R^2	**0.993**	*0.990*	0.993	0.992
RMSE	**0.0144**	*0.0173*	0.0146	0.0154
AIC (x1000)	**-1.44**	*-1.34*	-1.43	-1.40
	Entisol - N = 240			
R^2	0.996	0.996	**0.996**	*0.992*
RMSE	0.0087	0.0087	**0.0081**	*0.0116*
AIC (x1000)	-1.72	-1.72	**-1.76**	*-1.57*
	Anthrosol - N = 238			
R^2	**0.992**	0.990	0.990	*0.988*
RMSE	**0.0075**	0.0084	0.0083	*0.0095*
AIC (x1000)	**-1.79**	-1.72	-1.74	*-1.66*
	Alfisol - N = 240			
R^2	0.982	*0.978*	**0.985**	0.983
RMSE	0.0126	*0.0140*	**0.0116**	0.0123
AIC (x1000)	-1.52	*-1.48*	**-1.57**	-1.54

For a given fitting parameter, the value in bold indicate the best and the value in italics the worst performance

between the minimum and maximum RMSE values was in the range 0.40–0.47 indicating soil type influenced the accuracy of water retention fitting by an average factor of approximately 2.3. In other words, soil characteristics dominated fitting quality, with model selection probably exerting a secondary influence.

Nevertheless, in selecting the SWRC fitting model, VGN and VGM models consistently performed better than VGB and KSG models. In particular, VGN yielded the best performance (R^2, RMSE, and AIC) in loam (Inceptisol_1, Entisol, and Alfisol) and clay loam (Inceptisol_2) soils, while VGM performed better in finer soils (Vertisol and Anthrosol). The VGB model was the worst in four soils (Inceptisol_1, Inceptisol_2, Vertisol, and Alfisol) and the KSG in the other two soils (Entisol and Anthrosol) (Table 2). These results indicate that VGN and VGM models are recommended across the textural range examined (Table 1), with VGN tending to perform better in relatively coarse soils with sand content greater than 30 %.

Model performance varied with pressure head, generally declining at increasing h (Fig. S3). For $h < 50$ cm, the performance of VGN, VGM, and KSG models were comparable, whereas the VGB model gave the worst predictions. At increasing h, the KSG model progressively worsened. The VGN model yielded the best results for $50 \leq h < 1000$ cm, even if its performance was comparable with that of VGM and VGB. At $h = 15000$ cm, only the VGN model yielded nRMSE < 0.06. These results indicate the KSG model could yield relatively worse predictions of the dry end of the SWRC compared to the van Genuchten-type models. Among the latter models, an unconstrained m parameter (VGN) is preferable as it yields generally better predictions than the constrained van Genuchten models (VGM and VGB).

3.2. Estimation of the inflection point SPQ indicators

The functional form of the model may influence both the position and the slope of the SWRC, thereby affecting the estimation of the inflection point SPQ indicators. This aspect, which has received limited attention in the existing literature was therefore investigated.

The location of the SWRC inflection point, as indicated by the mean values of h^* and θ_g^*, was variable among the different models and pairwise comparisons confirmed these differences as statistically relevant (Fig. 1 and Table S2). Depending on the considered SWRC fitting model, the mean value of the gravimetric water content at the inflection point varied from 0.27 to 0.33 g g^{-1}. These θ_g^* values corresponded to a variation of the mean pressure head values from 101 to 278 cm. Pairwise ART-based comparisons of the aligned means showed that these inflection point SPQ indicators differed among models (Fig. 1 and Table S2). For the considered soils, the choice of SWRC model produced noticeable shifts in θ_g^* and h^*, underscoring that model selection affects the estimated location of the inflection point even when the same underlying data are used (Fig. 1). The comparatively larger variability in VGN-derived estimates reflects its greater flexibility that considers estimation of five fitting parameters compared to the four fitting parameters of the other models, enabling a finer adaptation to differing water retention shapes. As a consequence of the constraint on m, shape parameters of the VGM, VGB and KSG models (i.e., n and σ) were generally well correlated with the corresponding scale parameters (α and h_m). For example, a significant linear relationship ($R^2 = 0.564$, $N = 120$) was found for the VGM model between n and the inverse of α which is related to the air entry pressure head [26]. Conversely, for the VGN model no statistical relationship was found between the two parameters.

The slope at the inflection point (S^*) and the derived pore-size distribution index (λ*) were relatively similar among the four considered SWRC models. Unlike the location indicators (h^* and θ_g^*), S^* and λ* did not show detectable differences among the four models (Fig. 1 and Table S2), although their mean values varied modestly in the order KSG < VGM < VGN < VGB for S^* and VGB < VGM < VGN < KSG for λ*. Independently of the SWRC fitting model, the estimated S^* values fell within the range $0.007 \leq S^* \leq 0.140$ usually considered for agricultural soils [11,12]. Effective porosity (Φ*), by contrast, strongly depended on the selected SWRC model with the VGN model yielding the highest variability, consistent with its greater flexibility in fitting the SWRC. As for the capacitive SPQ indicators, air capacity (AC) and plant available water content (PAWC) showed no statistical difference across models (Fig. 1 and Table S2).

Together, these results indicate that the choice of the SWRC fitting model strongly influenced the estimates of h^*, θ_g^*, and Φ* inflection point indicators, while S^*, λ*, and the capacitive metrics (AC and PAWC) were less affected by the model selection. In conclusion, although some indicators were not affected by the fitted model, a reliable estimate of these parameters require an accurate selection of the SWRC model to be fitted to experimental data. For the aim of investigating the effects of MP contamination, according to the results found in the previous section, the estimates of the inflection point indicators were obtained from the VGN model for Inceptisol_1, Inceptisol_2, Entisol and Alfisol and from the VGM model for Vertisol and Anthrosol.

3.3. Soil physical quality of control soils

Under uncontaminated conditions (i.e., microplastics concentration, MP = 0, Ctr), the mean values of pressure head at the inflection point (h^*) varied between 143 and 504 cm depending on the soil type (Fig. 2). Variability among the eight replicates was substantial for some soils, and no simple monotonic trend with the soil texture emerged. The two loam soils Inceptisol_1 and Alfisol -having approximately the same clay content- were characterized by largely different h^* values ($h^* = 504$ and 186 cm, respectively). The mean values of the gravimetric water content at the inflection point θ_g^* followed more closely the soil texture classification, with loam soils (Inceptisol_1 and Alfisol) showing lower θ_g^* values compared to finer soils (Inceptisol_2 and Vertisol) (Fig. 2). Nonetheless, soils having comparable clay content values such as Entisol and Anthrosol (i.e., $Cl = 20.9$ % and 23.4 %, respectively) showed very

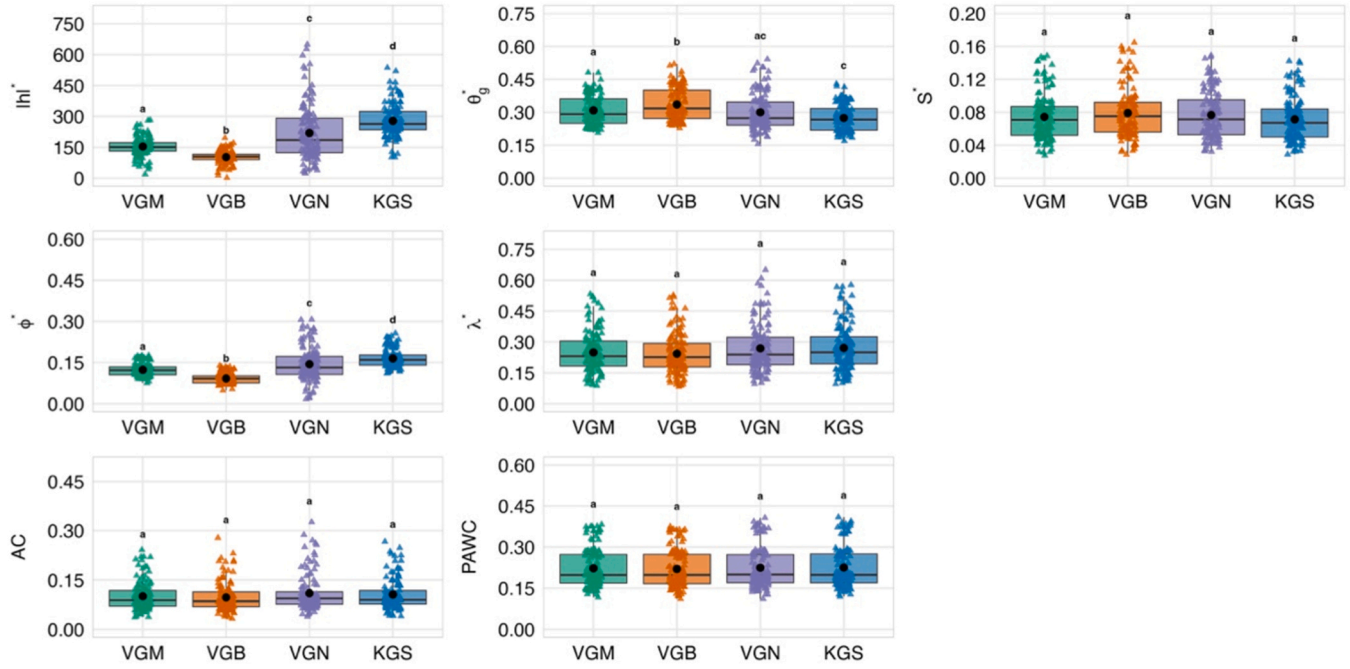

Fig. 1. Inflection (h^*, θ_g^*, S^*, Φ^*, λ^*) and capacitive (AC, PAWC) soil physical quality indicators estimated from the considered SWRC models. Data are presented as boxplots with coloured triangles indicating the datapoints and black central circles indicating the mean.

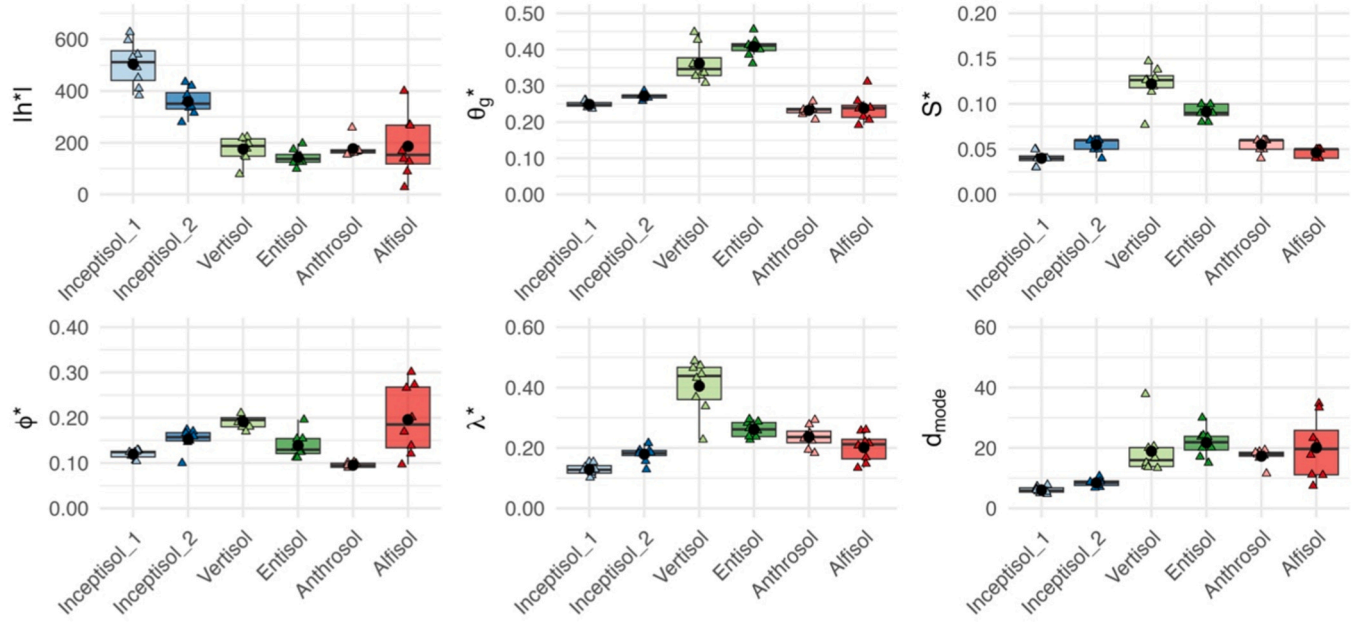

Fig. 2. Baseline variability of selected soil physical quality indicators (h^*, θ_g^*, S^*, Φ^*, λ^*) and modal pore equivalent diameter (d_{mode}) in uncontaminated control (Ctr) soils. Data are presented as boxplots with coloured triangles indicating the datapoints and black central circles indicating the mean.

different θ_g^* values ($\theta_g^* = 0.41$ and 0.24 g g^{-1}, respectively), underscoring that texture alone does not fully determine inflection-point location.

Effective saturation at the inflection point ($\Theta_g^* = (\theta_g^* - \theta_{gr})/(\theta_{gs} - \theta_{gr})$) showed a negative correlation with $\log(h^*)$ ($R^2 = 0.473$). Since h^* is linked to the inverse of the modal pore equivalent diameter, d_{mode}, by the capillary law [11], it can be concluded that as the size of the most frequent pores increases, the SWRC inflection point moves to relatively wetter conditions (Fig. 3a). The regression line for uncontaminated soils lie below the "optimal" soil proposed by Reynolds et al. [11] for rigid to moderately expansive agricultural soils ($\Theta_g^* = 0.76$; $h^* = 28$ cm). This result aligns with expectations given the use of repacked samples characterized predominantly by matrix pores of relatively narrow size.

The slope of the SWRC at the inflection point, S^*, varied substantially among the control soils (Table S3), ranging from 0.040 for Inceptisol_1 to 0.122 for Vertisol (Fig. 2). According to the existing criteria for S^* [11, 12], Inceptisol_1 and Alfisol under uncontaminated conditions exhibited "good" physical quality ($0.035 \leq S^* < 0.05$) while the other soils showed "very good" soil physical quality ($S^* \geq 0.05$). As expected, the slope of the SWRC at the inflection point, S^*, and the location of the inflection point were related. In particular, a low but significant positive regression was found between S^* and both d_{mode} and Θ_g^* ($R^2 = 0.297$

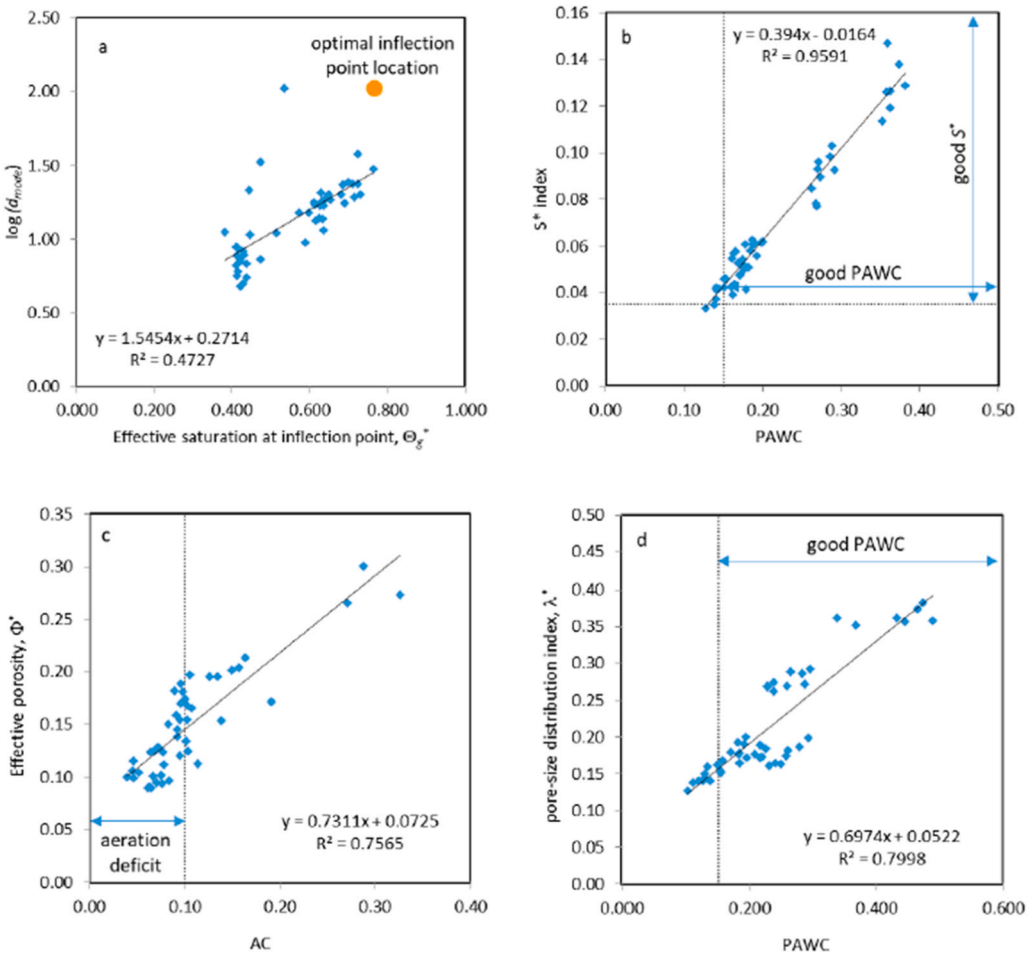

Fig. 3. Relationships between the inflection point and capacitive SPQ indicators of uncontaminated control (Ctr) soils: a) regression line between the logarithm of the modal diameter, d_{mode}, and the effective saturation at the inflection point, Θ_g*; b) regression line between slope of the soil water retention curve at the inflection point, S*, and the plant available water capacity, PAWC; c) Relationship between effective porosity, Φ*, and air capacity, AC; d) Relationship between pore size distribution index, λ*, and plant available water capacity, PAWC. Locations and ranges of recommended SPQ indicator values according existing literature criteria are also plotted (Agnese et al., [15]; Dexter and Czyz, [12]; Reynolds et al., [11]).

and 0.107, respectively) indicating that, as the inflection point shifts to lower pressure head (i.e., higher modal diameters) and higher effective saturation, the slope of the SWRC increases. This result is expected for water retention curves of well sorted soils that tend to be more sloped with an inflection point that occurs at low h* values (or large modal pore diameter). Vertisol (clay) and Entisol (loam) showed the highest mean values of S* (0.122 and 0.091, respectively) (Fig. 2) probably because the presence of microaggregates determined the formation of a "secondary" structure porosity during the incubation period which involved several wetting/drying cycles. Strong positive linear regression between S* and PAWC ($R^2 = 0.959$) confirmed pore size distribution's influence on SPQ (Fig. 3b). Most control samples fell within the good SPQ area defined by the existing literature criteria [11,12,15], with the regression line lying near the intersection of the two lines defining the lower boundaries of that good SPQ area.

The effective porosity, Φ*, varied with the soil type in a relatively small range of 0.10 cm^3cm^{-3} (i.e., from 0.095 to 0.195 cm^3cm^{-3} for Anthrosol and Alfisol, respectively) but no clear trend with the clay content was observed (Fig. 2). Furthermore, no correlation with the position (ln(h*) and Θ_g*) and the slope (S*) of the SWRC at the inflection point was found, indicating that Φ* can be considered as an independent parameter when assessing the SPQ. The pore-size distribution index, λ*, being functionally related to S*, followed the same trend with λ* values generally increasing with clay content ($R^2 = 0.854$ between λ* and S*). Since literature lacks Φ* and λ* thresholds for good SPQ, these were derived from correlations with established indicators (AC, PAWC). Based on traditional minimum AC of 0.10 cm^3cm^{-3} [15], and corresponding Φ* correlation ($R^2 = 0.757$) (Fig. 3c), good SPQ requires Φ* values larger than approximately 0.15 cm^3cm^{-3}. Following the same approach, the relationship between λ* and PAWC ($R^2 = 0.800$) (Fig. 3d) suggests that λ* > 0.15 indicates good quality. The existence of statistically significant regressions between Φ*, λ*, and the capacitive SPQ indicators (AC and PAWC) demonstrated that inflection point indicators yield SPQ estimates consistent with traditional capacitive, while establishing, for the first time, the ranges of Φ* and λ* for good soil physical conditions.

According to the established criteria for SPQ classification [11,12,15], the quality of the uncontaminated soils can be considered optimal with respect to the S* and PAWC indicators (Fig. 3b), but not when evaluated using AC values. Based on this indicator, 26 soil samples (54.2 % of the total) showed signs of limited aeration (Fig. 3c), and therefore their SPQ should be classified as degraded. The three-dimensional network of micro-cracks, fractures, and large inter-aggregate voids -which normally ensures adequate aeration under field conditions- is largely lost in repacked samples, explaining the low air capacity (AC) despite favourable values of SPQ indicators (S* and PAWC) that are mostly driven by matrix porosity.

3.4. Effects of microplastic contamination on SPQ indicators

ART-based ANOVA revealed detectable main effects of microplastic contamination, soil type, and their interaction on all investigated inflection point SPQ indicators (Table S4), with F-values of the main factor MP ranging from 6.38 for λ* to 51.44 for h^*, indicating varying sensitivity of different indicators to MP contamination.

Correlation analysis across all samples ($N = 120$) revealed dose-dependent relationships between PES MP concentration and SPQ indicators (Table 3). The pressure head at inflection point, h^*, showed the strongest negative correlation with MP concentration ($R = -0.443$), indicating progressive decreases in h^* with increasing contamination levels. Effective porosity, Φ*, also demonstrated a negative relationship ($R = -0.183$), while the slope parameter S^* exhibited a positive correlation ($R = 0.231$), suggesting enhanced aggregation with increasing PES MP loads. Notably, the gravimetric water content at inflection point, θ_g^*, showed a weaker positive correlation ($R = 0.207$), while of the two capacitive indicators, only AC displayed a minimal relationship with PES MP concentration (Table 3).

Soil-specific responses to PES MP contamination revealed marked heterogeneity in sensitivity patterns (Fig. 4 and Table 3). Moderate clay soils (Inceptisol_1, Inceptisol_2 and Entisol) exhibited the most pronounced responses, with correlations exceeding 0.60 for multiple indicators and mean h^* values that decreases up to 393 cm at 1 % w/w. Clay-rich Vertisol exhibited detectable correlations for h^* ($R = -0.742$) and θ_g^* ($R = 0.624$) but displayed a negative correlation for S^* ($R = -0.225$), suggesting potential deterioration rather than improvement in aggregation status. The silt loam Anthrosol showed moderate correlations across most indicators, with mean differences in Fig. 4 indicating gradual but consistent changes in h^* and S^* values. Notably, this soil uniquely displayed a positive correlation between PES MP concentration and Φ* ($R = 0.630$). Alfisol presented the most resistant profile, with effects limited primarily to aggregation-related parameters, S^* ($R = 0.855$) and λ* ($R = 0.742$). Strong effects predominantly occurred at 1 % w/w concentrations, with CIs at lower concentrations frequently including zero. Decreases in h^* were consistent across soils at all contamination levels, while S^* increases (0.01–0.04 units) occurred primarily in moderate clay soils.

Capacitive indicators (AC and PAWC) exhibited limited sensitivity to MP contamination, as evidenced by CIs frequently encompassing zero and low correlation coefficients (Fig. 4 and Table 3). This pattern suggests that the soil's bulk water retention capacity between key agronomic reference points (saturation, field capacity, and wilting point) remained substantially unaffected while PES MP contamination altered internal pore structure and aggregation characteristics. Specifically, a reduction in h^* indicates an increase in the most frequent pore diameter, suggesting PES MP contamination may have promoted the formation of larger pores likely due to enhanced particle aggregation facilitated by the fibrous nature of MPs. The observed reduction in Φ* coupled with decreased h^* values suggest a mechanism consistent with partial pore clogging by fibers creating fewer but larger conducting pores, as hypothesized by Neubert et al. [44]. The enhanced aggregation in contaminated soils is further confirmed by the increased S^* which, as proposed by Dexter [8], reflects a greater proportion of structural pores relative to those governed by texture.

Using Han et al. [62] empirical model ($K_s = C^* \Phi^{*3-\lambda^*}$) estimated K_s for contaminated samples ($K_s = 10.1$ mm/h) differed by a not significant 8 % from the control samples ($K_s = 9.4$ mm/h). This result is not surprising given that the increase in the size of the most frequent pores is counterbalanced by a reduction of the effective porosity, i.e., the volume of pores spanning from saturation to SWRC inflection point (Table 3). This structural rearrangement provides a physical explanation for the contrasting effects on hydraulic conductivity reported by Neubert et al. [44], where the net outcome (pore enlargement or connectivity loss) is ultimately determined by soil texture, leading to either increased or decreased water flow.

While SWRC-based analysis provides insights into water storage and pore structure, it does not directly characterize dynamic hydrological processes such as unsaturated hydraulic conductivity, infiltration rates, or solute transport. *S*-theory* establishes empirical relationships between inflection point indicators and dynamic properties, but direct verification of these relationships under MP contamination requires dedicated measurements. Our findings demonstrate that SWRC-derived indicators provide sensitive diagnostics for detecting MP-induced structural changes and identifying texture-specific vulnerability patterns. This information is essential for monitoring programs and risk assessment, but comprehensive management prescriptions and field-scale predictions of MP contamination effects require additional dynamic characterization.

Soils with moderate clay content and suboptimal potential structure (Inceptisol_1, Inceptisol_2) showed the greatest responsiveness to PES MP induced changes, while soils with very high clay content (Vertisol) exhibited more selective responses, suggesting the existence of an optimal textural range for PES MP soil interactions. These findings align with the emerging consensus that the effects of MPs are strongly mediated by soil texture and related properties [34,43,44,63,64]. Consequently, agronomic risk assessments must be soil-specific rather than based on universal thresholds.

Beyond hydraulic properties, the observed pore restructuring reveals a complex interplay between physical structure and functional outcomes. In a previous experiment using the same Entisol soil evaluated here, Ingraffia et al. [35] observed significant root biomass reductions and increased nitrogen leaching under PES contamination. These negative plant responses occurred despite the soil maintaining adequate water storage capacity, as demonstrated in the present study through preserved AC and PAWC values. This indicates that pore structural changes -particularly the reduction in effective porosity (Φ*) creating fewer total pores despite larger individual pore sizes- affect root exploration space, gas diffusion, and preferential flow pathways in ways not captured by traditional capacitive indicators. Changes in pore architecture also affect microbial communities, as pore size distribution critically determines habitat availability and substrate accessibility [65], potentially altering decomposition and nutrient cycling processes.

The dose-response patterns observed suggest minimal MPs effects on soil physical properties under current environmental contamination levels, (most changes occurred at 1 % w/w). However, Meizoso-Regueira et al. [46] forecast contamination levels may increase substantially, potentially reaching ~0.7 % within the next century.

Table 3
Correlation coefficients between soil physical quality indicators and microplastic concentration for the full dataset (All) and by soil type.

	N	h^*	θ_g^*	S^*	Φ*	λ*	AC	PAWC
All	120	**-0.443**	**0.207**	**0.231**	**-0.183**	0.152	**0.218**	0.042
Inceptisol_1	20	**-0.798**	**0.727**	**0.696**	**-0.515**	0.594	**0.668**	**0.499**
Inceptisol 2	20	**-0.825**	**0.749**	**0.652**	**-0.484**	0.202	0.107	0.331
Vertisol	20	**-0.742**	**0.624**	-0.225	-0.280	-0.242	**0.792**	**-0.432**
Entisol	20	**-0.751**	**0.744**	0.421	**-0.768**	-0.075	0.165	-0.161
Anthrosol	20	-0.442	0.297	**0.468**	**0.630**	0.275	**0.714**	0.305
Alfisol	20	-0.096	-0.168	**0.855**	-0.155	**0.742**	0.079	**0.637**

Boldface indicates $P < 0.05$.

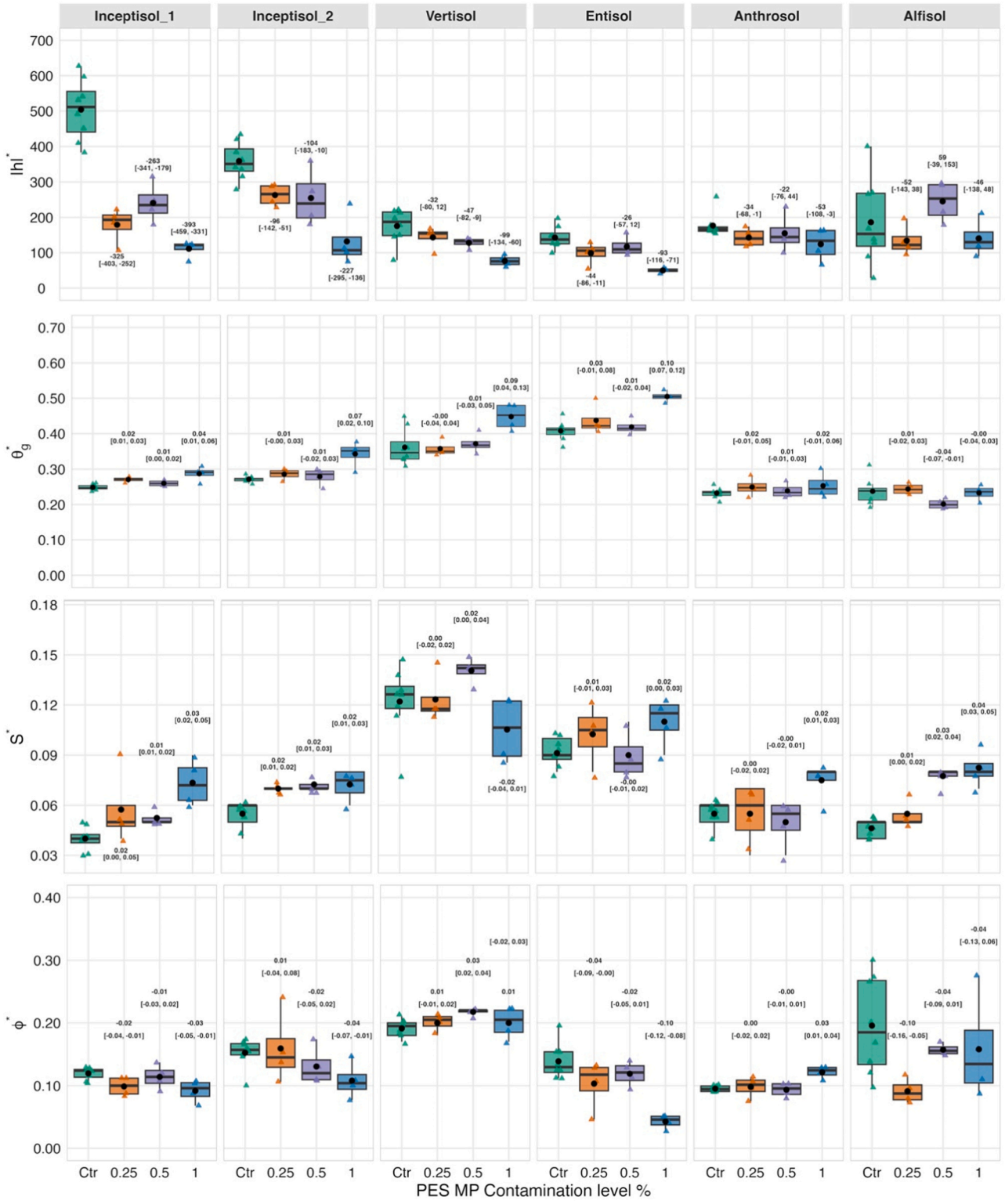

Fig. 4. Effects of polyester microplastic fiber contamination on the selected inflection (h^*, θ_g^*, S^*, Φ^*, λ^*) and capacitive (AC, PAWC) soil physical quality indicators. Data are presented as boxplots with coloured triangles indicating the datapoints and black central circles indicating the mean. The mean difference between each microplastic treatment and the control within each soil type is reported above each box, while the accelerated bootstrap 95 % confidence intervals are reported below the corresponding mean difference.

4. Conclusions

This study provides the first comprehensive assessment of polyester microplastic fiber effects on soil physical quality using inflection point indicators derived from soil water retention curves. Our investigation reveals that the van Genuchten model with unconstrained parameters (VGN) and the Mualem-constrained version (VGM) consistently outperformed other soil water retention curve models across diverse soil

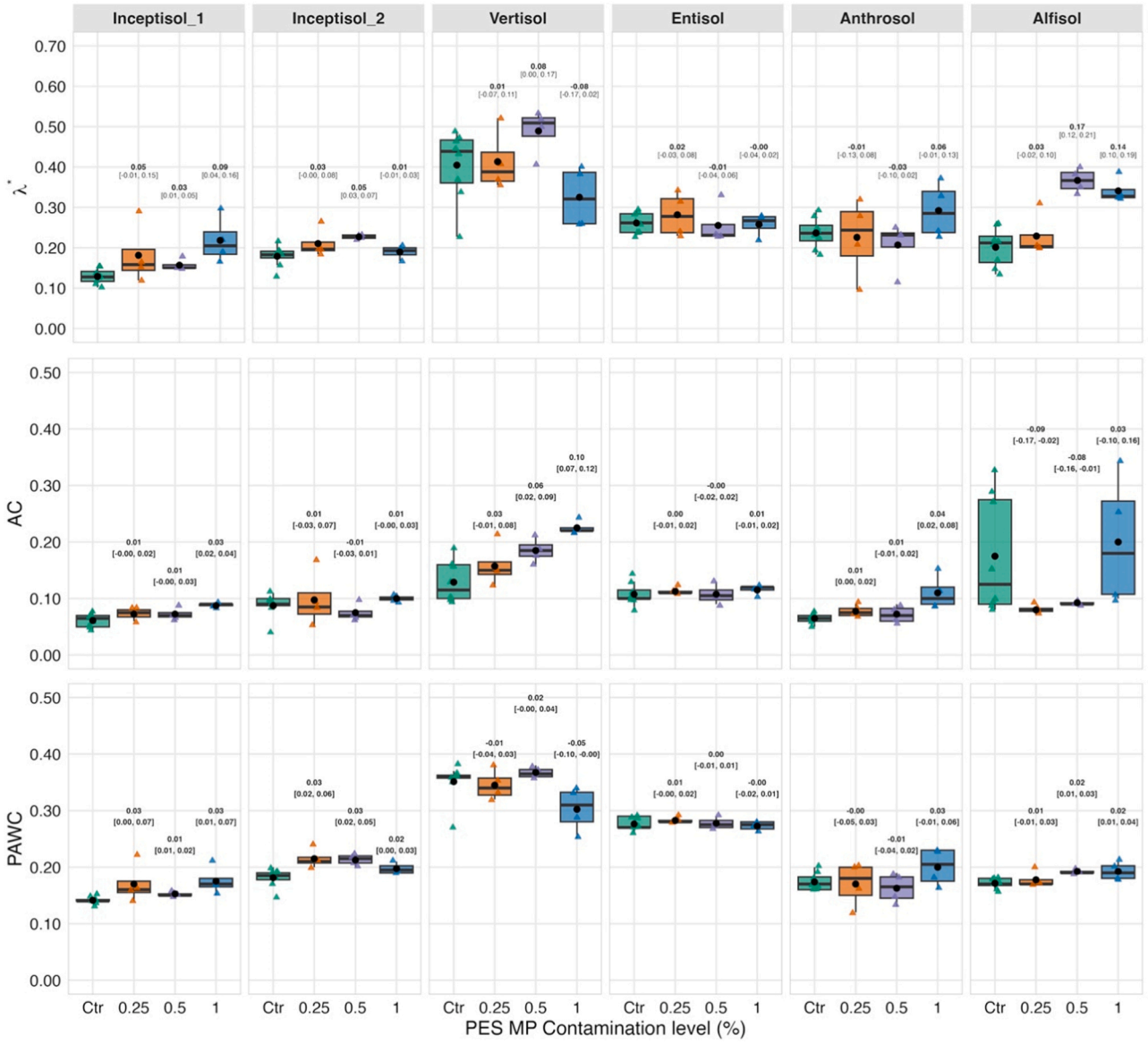

Fig. 4. (*continued*).

textures. The choice of model strongly influenced the estimation of inflection point location parameters (h^* and θ_g^*) and effective porosity (Φ^*), while slope-related parameters (S^* and λ^*) showed lower model dependence, emphasizing the importance of appropriate model selection for reliable soil physical quality assessment.

PES MP contamination substantially altered soil pore architecture, decreasing pressure heads at inflection points, h^*, by up to 393 cm in moderate-clay soils while increasing slope, S^*, values by 0.01–0.04 units. The magnitude and direction of MP effects varied considerably among soil types, with soils containing moderate clay content (Clay $<$ 30 %) showing the greatest improvements in S^* values. Clay-rich soils, already exhibiting near-optimal physical quality, showed limited response to PES MP addition. This differential sensitivity highlights the importance of considering soil texture and initial physical quality when assessing MP impacts.

The preservation of capacitive indicators (AC and PAWC) despite changes in pore structure suggests that PES MP fibers modify internal pore geometry without substantially altering porosity between key agronomic reference points (saturation, field capacity, and permanent wilting point). The observed structural rearrangement, highlighted by changes in Φ^* and λ^*, indicates that the primary hazard may not be a loss of water storage, but a destabilization of the soil's water flow dynamics, potentially increasing risks of preferential flow and pollutant leaching, though direct verification of these effects requires dedicated measurements of the soil hydrodynamic properties that were beyond the scope of this study. The influence of PES MP fibers contamination on the near saturated soil hydraulic conductivity of the selected soils is the subject of ongoing investigation.

Most detectable effects occurred at the highest PES MP concentration (1 % w/w), suggesting the existence of contamination thresholds below which SPQ modifications remain minimal. This finding has important implications for establishing soil quality guidelines and contamination limits in agricultural systems.

This study was conducted on repacked soil samples under controlled conditions, which may not fully represent field conditions where soil structure, biological activity, and environmental variability play crucial roles. Future research should address long-term effects under field conditions, interactions between MPs and other soil amendments, impacts on biological processes and plant-soil interactions, and evaluation of remediation strategies. Overall, our findings suggest that agricultural management implications include the need for soil-specific risk assessments rather than universal contamination thresholds, enhanced

monitoring of plastic inputs in agricultural systems, and development of soil-type-specific remediation strategies prioritizing soils most vulnerable to negative impacts.

Environmental implication

The most detectable effects of PES MP fiber contamination occurred at 1 % w/w concentration, with minimal structural changes at lower levels. This concentration-dependent response suggests the existence of a threshold behavior in MP-soil interactions. SWRC-derived inflection point indicators (h^*, Φ^*, and S^*) proved sensitive to PES-induced structural modifications even when capacitive indicators (AC and PAWC) remained unchanged. The effects varied with soil texture, with moderate-clay soils (<30 %) exhibiting the most pronounced responses, while clay-rich soils showed minimal structural changes. These texture-specific patterns indicate that MP effects depend critically on soil properties. Monitoring and risk assessment strategies should therefore account for soil type rather than applying universal contamination thresholds.

CRediT authorship contribution statement

Rosolino Ingraffia: Writing – review & editing, Writing – original draft, Investigation, Formal analysis. **Cristina Bondì:** Writing – review & editing, Data curation. **Dario Autovino:** Writing – review & editing, Data curation. **Dario Giambalvo:** Writing – review & editing, Conceptualization. **Paolo Ruisi:** Writing – review & editing, Data curation. **Vincenzo Bagarello:** Writing – review & editing, Conceptualization. **Massimo Iovino:** Writing – review & editing, Writing – original draft, Validation, Formal analysis, Conceptualization.

Funding

The authors acknowledge funding from the University of Palermo (Palermo, Italy).

Declaration of Competing Interest

The authors declare that they have no known competing financial interests or personal relationships that could have appeared to influence the work reported in this paper.

Appendix A. Supporting information

Supplementary data associated with this article can be found in the online version at doi:10.1016/j.jhazmat.2026.141549.

Data availability

Data will be made available on request.

References

[1] Reynolds, W.D., Bowman, B.T., Drury, C.F., Tan, C.S., Lu, X., 2002. Indicators of good soil physical quality: density and storage parameters. Geoderma 110, 131–146. https://doi.org/10.1016/S0016-7061(02)00228-8.
[2] Topp, G.C., Reynolds, W.D., Cook, F.J., Kirby, J.M., Carter, M.R., 1997. Physical attributes of soil quality. Developments in Soil Science. Elsevier, pp. 21–58.
[3] Reynolds, W.D., Drury, C.F., Yang, X.M., Tan, C.S., 2008. Optimal soil physical quality inferred through structural regression and parameter interactions. Geoderma 146, 466–474. https://doi.org/10.1016/j.geoderma.2008.06.017.
[4] Abel, S., Peters, A., Trinks, S., Schonsky, H., Facklam, M., Wessolek, G., 2013. Impact of biochar and hydrochar addition on water retention and water repellency of sandy soil. Geoderma 202-203, 183–191. https://doi.org/10.1016/j.geoderma.2013.03.003.
[5] Di prima, S., Rodrigo-comino, J., Novara, A., Iovino, M., Pirastru, M., Keesstra, S., et al., 2018. Soil physical quality of citrus orchards under tillage, herbicide, and organic managements. Pedosphere 28, 463–477. https://doi.org/10.1016/S1002-0160(18)60025-6.
[6] Drewry, J.J., Cameron, K.C., Buchan, G.D., 2008. Pasture yield and soil physical property responses to soil compaction from treading and grazing—a review. Aust J Soil Res 46, 237–256. https://doi.org/10.1071/SR07125.
[7] Reynolds, W.D., Drury, C.F., Yang, X.M., Fox, C.A., Tan, C.S., Zhang, T.Q., 2007. Land management effects on the near-surface physical quality of a clay loam soil. Soil Tillage Res 96, 316–330. https://doi.org/10.1016/j.still.2007.07.003.
[8] Dexter, A.R., 2004. Soil physical quality: Part I. Theory, effects of soil texture, density, and organic matter, and effects on root growth. Geoderma 120, 201–214. https://doi.org/10.1016/j.geoderma.2003.09.004.
[9] Dexter, A.R., 2004. Soil physical quality: Part II. Friability, tillage, tilth and hard-setting. Geoderma 120, 215–225. https://doi.org/10.1016/j.geoderma.2003.09.005.
[10] Dexter, A.R., 2004. Soil physical quality: Part III: Unsaturated hydraulic conductivity and general conclusions about S-theory. Geoderma 120, 227–239. https://doi.org/10.1016/j.geoderma.2003.09.006.
[11] Reynolds, W.D., Drury, C.F., Tan, C.S., Fox, C.A., Yang, X.M., 2009. Use of indicators and pore volume-function characteristics to quantify soil physical quality. Geoderma 152, 252–263.
[12] Dexter, A.R., Czyż, E.A., 2007. Applications of S-theory in the study of soil physical degradation and its consequences. Land Degrad Dev 18, 369–381. https://doi.org/10.1002/ldr.779.
[13] Dexter, A.R., Bird, N.R.A., 2001. Methods for predicting the optimum and the range of soil water contents for tillage based on the water retention curve. Soil Tillage Res 57, 203–212. https://doi.org/10.1016/S0167-1987(00)00154-9.
[14] Tormena, C.A., Silva, Á.P. da, Imhoff, S.D.C., Dexter, A.R., 2008. Quantification of the soil physical quality of a tropical oxisol using the S index. Sci Agric 65, 56–60. https://doi.org/10.1590/S0103-90162008000100008.
[15] Agnese, C., Bagarello, V., Baiamonte, G., Iovino, M., 2011. Comparing physical quality of forest and pasture soils in a Sicilian watershed. Soil Sci Soc Am J 75, 1958–1970. https://doi.org/10.2136/sssaj2011.0044.
[16] Castellini, M., Niedda, M., Pirastru, M., Ventrella, D., 2014. Temporal changes of soil physical quality under two residue management systems. Soil Use Manag 30, 423–434. https://doi.org/10.1111/sum.12137.
[17] Chakraborty, D., Garg, R.N., Tomar, R.K., Dwivedi, B.S., Aggarwal, P., Singh, R., et al., 2010. Soil physical quality as influenced by long-term application of fertilizers and manure under maize-wheat system. Soil Sci 175, 128. https://doi.org/10.1097/SS.0b013e3181d53bd7.
[18] Iovino, M., Castellini, M., Bagarello, V., Giordano, G., 2016. Using static and dynamic indicators to evaluate soil physical quality in a Sicilian area. Land Degrad Dev 27, 200–210. https://doi.org/10.1002/ldr.2263.
[19] Satriani, A., Belviso, C., Lovelli, S., di Prima, S., Coppola, A., Hassan, S.B.M., et al., 2024. Impact of a synthetic zeolite mixed with soils of different pedological characteristics on soil physical quality indices. Geoderma 451, 117084. https://doi.org/10.1016/j.geoderma.2024.117084.
[20] Li, L., Chan, K.Y., Niu, Y., Li, G., Oates, A., Dexter, A., et al., 2011. Soil physical qualities in an Oxic Paleustalf under different tillage and stubble management practices and application of S theory. Soil Tillage Res 113, 82–88. https://doi.org/10.1016/j.still.2011.02.007.
[21] Nascimento, D.M. do, Cavalieri-Polizeli, K.M.V., Silva, A.H. da, Favaretto, N., Parron, L.M., 2019. Soil physical quality under long-term integrated agricultural production systems. Soil Tillage Res 186, 292–299. https://doi.org/10.1016/j.still.2018.08.016.
[22] Silva, G.L., Lima, H.V., Campanha, M.M., Gilkes, R.J., Oliveira, T.S., 2011. Soil physical quality of Luvisols under agroforestry, natural vegetation and conventional crop management systems in the Brazilian semi-arid region. Geoderma 167168 61–70. https://doi.org/10.1016/j.geoderma.2011.09.009.
[23] Ibraheem, T., Hajabbasi, M.A., Shariatmadari, H., 2024. Effects of biochar and municipal solid waste compost on soil physical quality and productivity index under sorghum cultivation irrigated with saline water. Commun Soil Sci Plant Anal 55, 1476–1487. https://doi.org/10.1080/00103624.2024.2319799.
[24] He, Y., Song, X., Li, X., Gao, Y., Yang, J., Chen, J., et al., 2023. Spatial properties of soil physical quality index S in black soil croplands under permanent gully erosion. Land 12, 1641. https://doi.org/10.3390/land12091641.
[25] Arthur, E., Cornelis, W.M., Vermang, J., De Rocker, E., 2011. Amending a loamy sand with three compost types: impact on soil quality. Soil Use Manag 27, 116–123. https://doi.org/10.1111/j.1475-2743.2010.00319.x.
[26] Bondì, C., Castellini, M., Iovino, M., 2022. Compost amendment impact on soil physical quality estimated from hysteretic water retention curve. Water 14, 1002. https://doi.org/10.3390/w14071002.
[27] Bondì, C., Castellini, M., Iovino, M., 2025. Temporal variability of physical quality of a sandy loam soil amended with compost. Biologia 80, 1221–1232. https://doi.org/10.1007/s11756-024-01637-1.
[28] Głąb, T., Żabiński, A., Sadowska, U., Gondek, K., Kopeć, M., Mierzwa–Hersztek, M., et al., 2018. Effects of co-composted maize, sewage sludge, and biochar mixtures on hydrological and physical qualities of sandy soil. Geoderma 315, 27–35. https://doi.org/10.1016/j.geoderma.2017.11.034.
[29] van Genuchten, M.Th, 1980. A closed-form equation for predicting the hydraulic conductivity of unsaturated soils. Soil Sci Soc Am J 44, 892–898. https://doi.org/10.2136/sssaj1980.03615995004400050002x.
[30] Kosugi, K., 1994. Three-parameter lognormal distribution model for soil water retention. Water Resour Res 30, 891–901. https://doi.org/10.1029/93WR02931.
[31] Rastgou, M., He, Y., Wang, J., Bayat, H., Shao, M., Li, Y., et al., 2023. A technical evaluation on the mathematical attitudes and fitting accuracy of soil moisture retention curve models. Comput Electron Agric 215, 108347. https://doi.org/10.1016/j.compag.2023.108347.

[32] Hartmann, N.B., Hüffer, T., Thompson, R.C., Hassellöv, M., Verschoor, A., Daugaard, A.E., et al., 2019. Are we speaking the same language? recommendations for a definition and categorization framework for plastic debris. Environ Sci Technol 53, 1039–1047. https://doi.org/10.1021/acs.est.8b05297.
[33] Guo, Z., Li, P., Yang, X., Wang, Z., Lu, B., Chen, W., et al., 2022. Soil texture is an important factor determining how microplastics affect soil hydraulic characteristics. Environ Int 165, 107293. https://doi.org/10.1016/j.envint.2022.107293.
[34] Ingraffia, R., Amato, G., Bagarello, V., Carollo, F.G., Giambalvo, D., Iovino, M., et al., 2022. Polyester microplastic fibers affect soil physical properties and erosion as a function of soil type. SOIL 8, 421–435. https://doi.org/10.5194/soil-8-421-2022.
[35] Ingraffia, R., Amato, G., Iovino, M., Rillig, M., Giambalvo, D., Frenda, A.S., 2022. Polyester microplastic fibers in soil increase nitrogen loss via leaching and decrease plant biomass production and N uptake. Environ Res Lett. https://doi.org/10.1088/1748-9326/ac652d.
[36] Lozano, Y.M., Lehnert, T., Linck, L.T., Lehmann, A., Rillig, M.C., 2021. Microplastic shape, polymer type, and concentration affect soil properties and plant biomass. Front Plant Sci 12. https://doi.org/10.3389/fpls.2021.616645.
[37] de Souza Machado, A.A., Lau, C.W., Till, J., Kloas, W., Lehmann, A., Becker, R., et al., 2018. Impacts of microplastics on the soil biophysical environment. Environ Sci Technol 52, 9656–9665. https://doi.org/10.1021/acs.est.8b02212.
[38] Sahai, H., Aguilera del Real, A.M., Alcayde, A., Bueno, M.J.M., Wang, C., Hernando, M.D., et al., 2025. Key insights into microplastic pollution in agricultural soils: A comprehensive review of worldwide trends, sources, distribution, characteristics and analytical approaches. TrAC Trends Anal Chem 185, 118176. https://doi.org/10.1016/j.trac.2025.118176.
[39] Yang, J., Li, L., Li, R., Xu, L., Shen, Y., Li, S., et al., 2021. Microplastics in an agricultural soil following repeated application of three types of sewage sludge: A field study. Environ Pollut 289, 117943. https://doi.org/10.1016/j.envpol.2021.117943.
[40] Zhou, B., Wang, J., Zhang, H., Shi, H., Fei, Y., Huang, S., et al., 2020. Microplastics in agricultural soils on the coastal plain of Hangzhou Bay, east China: multiple sources other than plastic mulching film. J Hazard Mater 388, 121814. https://doi.org/10.1016/j.jhazmat.2019.121814.
[41] La, Y., Zhang, L., Zhao, N., Ye, H., Zeng, Q., Zhao, L., et al., 2024. The microplastics distribution characteristics and their impact on soil physicochemical properties and bacterial communities in food legumes farmland in northern China. J Hazard Mater 471, 134282. https://doi.org/10.1016/j.jhazmat.2024.134282.
[42] Kärkkäinen, N., Selonen, S., Hartonen, K., Sillanpää, M., 2025. Microplastic pollution via wastewater effluent and sewage sludge: special focus on microplastic fibres in compost. Water Air Soil Pollut 236, 911. https://doi.org/10.1007/s11270-025-08563-1.
[43] Chen, H., Ingraffia, R., Schloter, M., Brüggemann, N., Rillig, M.C., 2025. Effects of multiple microplastic types on growth of winter wheat and soil properties vary in different agricultural soils. Plants People Planet 7, 194–203. https://doi.org/10.1002/ppp3.10573.
[44] Neubert, K.J., Weihermüller, L., Vereecken, H., Brüggemann, N., 2025. Soil texture governs the influence of different microplastics on soil hydraulic properties. Vadose Zone J 24, e70044. https://doi.org/10.1002/vzj2.70044.
[45] Zhang, G.S., Zhang, F.X., Li, X.T., 2019. Effects of polyester microfibers on soil physical properties: perception from a field and a pot experiment. Sci Total Environ 670, 1–7. https://doi.org/10.1016/j.scitotenv.2019.03.149.
[46] Meizoso-Regueira, T., Fuentes, J., Cusworth, S.J., Rillig, M.C., 2024. Prediction of future microplastic accumulation in agricultural soils. Environ Pollut 359, 124587. https://doi.org/10.1016/j.envpol.2024.124587.
[47] Dazzi, C., Galati, A., Crescimanno, M., Lo Papa, G., 2019. Pedotechnique applications in large-scale farming: economic value, soil ecosystems services and soil security. CATENA 181, 104072. https://doi.org/10.1016/j.catena.2019.104072.
[48] Gee, G.W., Or, D., 2002. 2.4 particle-size analysis. Methods of Soil Analysis. John Wiley & Sons, Ltd, pp. 255–293.
[49] Chia, R.W., Lee, J.-Y., Jang, J., Kim, H., Kwon, K.D., 2022. Soil health and microplastics: a review of the impacts of microplastic contamination on soil properties. J Soils Sediment 22, 2690–2705. https://doi.org/10.1007/s11368-022-03254-4.
[50] Dane, J.H., Hopmans, J.W., Topp, G.C., 2002. Hanging water column. Methods of Soil Analysis Part 4, pp. 680–683.
[51] Dane, J.H., Hopmans, J.W., Topp, G.C., 2002. Pressure plate extractor. Methods of Soil Analysis Part 4, pp. 688–690.
[52] Mualem, Y., 1976. A new model for predicting the hydraulic conductivity of unsaturated porous media. Water Resour Res 12, 513–522. https://doi.org/10.1029/WR012i003p00513.
[53] Burdine, N.T., 1953. Relative permeability calculations from pore size distribution data. J Pet Technol 5, 71–78. https://doi.org/10.2118/225-G.
[54] Fredlund, D.G., Xing, A., 1994. Equations for the soil-water characteristic curve. Can Geotech J 31, 521–532. https://doi.org/10.1139/t94-061.
[55] Castellini, M., Bondì, C., Giglio, L., Iovino, M., 2024. Impact of vermicompost addition on water availability of differently textured soils. Heliyon 10. https://doi.org/10.1016/j.heliyon.2024.e35699.
[56] Lilliefors, H.W., 1967. On the Kolmogorov-Smirnov test for normality with mean and variance unknown. J Am Stat Assoc 62, 399–402. https://doi.org/10.1080/01621459.1967.10482916.
[57] Kay, M., Elkin, L.A., Higgins, J.J., Wobbrock, J.O., 2021. ARTool: Aligned Rank Transform.
[58] Canty, A., Ripley, B., 2025. boot: Bootstrap Functions.
[59] Wickham, H., Averick, M., Bryan, J., Chang, W., McGowan, L.D., François, R., et al., 2019. Welcome to the tidyverse. J Open Source Softw 4, 1686. https://doi.org/10.21105/joss.01686.
[60] Wickham, H., 2016. ggplot2: Elegant Graphics for Data Analysis. Springer.
[61] R Core Team, 2024. R: A Language and Environment for Statistical Computing_. R Foundation for Statistical Computing, Vienna, Austria. ⟨https://www.R-project.org/⟩.
[62] Han, H., Giménez, D., Lilly, A., 2008. Textural averages of saturated soil hydraulic conductivity predicted from water retention data. Geoderma 146, 121–128. https://doi.org/10.1016/j.geoderma.2008.05.017.
[63] Lo Porto, A., Amato, G., Gargano, G., Giambalvo, D., Ingraffia, R., Torta, L., et al., 2024. Polypropylene microfibers negatively affect soybean growth and nitrogen fixation regardless of soil type and mycorrhizae presence. J Hazard Mater 480, 135781. https://doi.org/10.1016/j.jhazmat.2024.135781.
[64] Lammel, D.R., Kim, S.W., Rong, L., Chen, H., Ingraffia, R., Rillig, M.C., 2025. Effects of microplastic types and shapes on the community structure of arbuscular mycorrhizal fungi in different soil types. Environ Sci Pollut Res 32, 12504–12512. https://doi.org/10.1007/s11356-025-36408-1.
[65] Han, L., Chen, L., Feng, Y., Kuzyakov, Y., Chen, Q., Zhang, S., et al., 2024. Microplastics alter soil structure and microbial community composition. Environ Int 185, 108508. https://doi.org/10.1016/j.envint.2024.108508.